*Short Communication*

# Effect of a High Concentration of Chloride Ions on the Corrosion Behaviour of X80 Pipeline Steel in 0.5 mol L$^{-1}$ NaHCO$_3$ Solutions

*Wen Zhou, Wei Lan*, Xianlong Cao*, Hongda Deng, Yongbo Yan, Xianglong Hou*

School of Metallurgy and Materials Engineering, Chongqing University of Science and Technology, Chongqing 401331, China
*E-mail: ckffyjs@163.com, caoxianlong318@163.com

A dynamic potential polarization technique and electrochemical impedance spectroscopy (EIS) measurements were used to explore the effects of a high concentration of chloride ions on the electrochemical corrosion properties of X80 pipeline steel in 0.5 mol L$^{-1}$ NaHCO$_3$ solutions. The surface corrosion morphology of X80 steel after polarization measurements was observed by scanning electron microscopy (SEM). The electrochemical results showed that the corrosion-product resistance and charge-transfer resistance decrease gradually with the increase of chloride ions, which resulted in the corrosion current density increasing monotonically. The surface corrosion morphology showed no pit formation in 0.5 mol L$^{-1}$ NaHCO$_3$ solutions without chloride ions. However, the addition of chloride ions decreases the stability of the passive film, and the density, size and depth of the corrosion pits increased with the increasing concentrations of chloride ions. Therefore, high concentrations of chloride ions greatly affected the electrochemical characteristics and caused further development of pitting in 0.5 mol L$^{-1}$ NaHCO$_3$ solutions.

## 1. INTRODUCTION

X80 pipeline steel is a low-carbon, micro-alloyed, high-grade steel, which has become one of the major steels used for building the gas transmission pipelines in China's "West-East" project [1, 2]. This is mainly due to the characteristics of X80 steel with its high-strength and high toughness, good weldability, and low ductile-to-brittle transition temperature [3, 4]. However, when pipeline steel is buried underground, the actual service life of pipeline steel is reduced due to the corrosive action of HCO$_3^-$, Cl$^-$ and SO$_4^{2-}$ ions in the soil [5, 6]. In particular, chloride ions can not only induce and activate

the X80 surface but also contribute to the rupture of the oxide/hydroxide film, resulting in severe pitting corrosion on the surface of X80 steel [7, 8].

Until now, a number of experiments have been conducted to research the corrosion of pipeline steel in carbonate-bicarbonate-sulfate-chloride solutions [7, 9, 10]. Zeng et al. [11] performed a study of X70 pipeline steel in 0.5 mol L$^{-1}$ NaHCO$_3$ solutions. This research found that the corrosion product film on X70 is primarily composed of an inner layer of Fe$_3$O$_4$ and an outer layer of γ-Fe$_2$O$_3$. Furthermore, they found that the corrosion product film became thinner in low chloride ion-concentration solutions. However, the electrochemical corrosion reaction process of the pipeline steel in 0.5 mol L$^{-1}$ NaHCO$_3$ solutions with different concentrations of chloride ions was not studied in their work. Wang et al. [7] proposed a mechanism for the initiation and propagation processes of pitting corrosion of X80 steel in sodium chloride solutions. Although a large number of studies have been performed to clarify the corrosion behaviour of pipeline steel in highly concentrated HCO$_3^-$, SO$_4^{2-}$ and CO$_3^{2-}$ solutions, research on the corrosion of X80 in HCO$_3^-$ solutions with high concentrations of chloride ions has been less emphasized [12, 13]. Therefore, to ensure the safety of X80 pipeline steel in service, the electrochemical properties of X80 pipeline steel exposed to bicarbonate–chloride environments should be investigated.

Based on this information, the purpose of this work was to investigate the electrochemical properties of X80 in 0.5 mol L$^{-1}$ NaHCO$_3$ solutions with different concentrations of chloride ions and the corrosion morphology of the steel after polarization to examine the effects of chloride ions on the corrosion behaviour of X80 pipeline steel in 0.5 mol L$^{-1}$ NaHCO$_3$ solutions.


## 2. EXPERIMENTAL

### 2.1 Preparation of the specimens and solutions

The X80 pipeline steel used in the experiment was cut into 25 mm × 20 mm × 15 mm samples with a wire cutting machine. Its chemical composition (wt. %) is shown in Table 1. Prior to each group of experiments, all sample surfaces were sequentially ground to 1500$^{\#}$ with continuous-sheet, fine-grade SiC water sandpaper, rinsed with acetone, washed with deionized water, degreased with absolute ethanol for 10 mins, and then dried with cold compressed air and placed in a desiccator.


**Table 1.** Chemical composition of X80（wt. %）

| C | Mn | P | S | Si | Nb | Cr | Ni | Ti | Mo | Fe |
|------|------|-------|-------|-------|-------|-------|-------|-------|-------|------|
| 0.079 | 1.50 | 0.023 | 0.007 | 0.274 | 0.019 | 0.067 | 0.131 | 0.015 | 0.324 | Bal. |


In this study, the corrosion solution was composed of deionized water and analytical reagent-grade NaCl and NaHCO$_3$. The base for the corrosive solutions was 0.5 mol L$^{-1}$ NaHCO$_3$, and different concentrations of NaCl were added to prepare the experimental solutions. The concentrations of Cl$^-$ used in the corrosion solutions were 0.1 mol L$^{-1}$, 0.2 mol L$^{-1}$, 0.3 mol L$^{-1}$, and 0.4 mol L$^{-1}$. A 0.5 mol L$^-$

[1] $NaHCO_3$ solution without chloride was used as a comparative test. The experiments were carried out at room temperature ($18 \pm 2$ °C).

## 2.2. Electrochemical measurements

All electrochemical tests were performed in a horizontal three-electrode glass jacket test cell with a total volume of 0.5 L, and the test sample was exposed to solutions across an area of 1 cm$^2$. The X80 sample was used as the working electrode with a platinum electrode as the counter electrode and a Ag/AgCl (3.5 mol L$^{-1}$ KCl) electrode as the reference electrode. A PARSTAT 4000A (Princeton, USA) electrochemical workstation was used for the open-circuit potential test (OCP), potential polarization curves test and electrochemical impedance spectroscopy (EIS). In this study, the stable potential of X80 was tested by an open-circuit potential test method (OCP) after immersion in corrosion solutions for 1 h. Electrochemical impedance spectroscopy testing was performed at an open circuit potential with a disturbance potential of 10 mV amplitude and a frequency range from 0.01 Hz to 10 KHz. The analysis of the AC impedance spectrum and fitting to equivalent circuits was performed using  ZsimpWin software. A potentiodynamic polarization curve test was performed by scanning the electrode potential with a scan rate of 1 mV s$^{-1}$ and a potential in the range of -1.0 V ~ 1.5 V. The corrosion morphology of the X80 sample after polarization was studied by S-3700N scanning electron microscopy (SEM) (Hitachi, Japan).
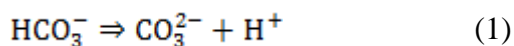
## 3. RESULTS AND DISCUSSION

### 3.1 Dynamic potential polarization curves

The polarization behaviour of X80 pipeline steel in 0.5 mol L$^{-1}$ $NaHCO_3$ solutions with different concentrations of chloride ions is shown in Figure 1. It can be seen from Figure 1 that the two anode current peaks (B, D) appeared in the anode polarization process when the 0.5 mol L$^{-1}$ $NaHCO_3$ solutions did not contain chloride ions. Lu [14] noted that there are two anodic current peaks in the anodic polarization curve of a 0.5 mol L$^{-1}$ $NaHCO_3$ solution, and the peak value of the second current is much lower than that of the first current curve, which is due to X80 exhibiting activation-passivation-transpassivation processes in $NaHCO_3$ solutions.
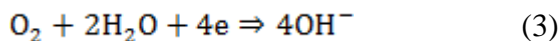
The activation of X80 mainly occurs in the AB segment, and the first anode current peak occurs at point B. With the increase of the anodic polarization potential, the corrosion current density of point B decreases gradually, which indicates that a corrosion product forms on the surface of the X80 specimen during the anodic polarization process. The possible electrochemical reactions contributing to this process are as follows [14-16]:

Bicarbonate ion dissociation:
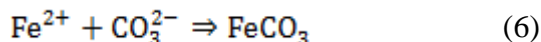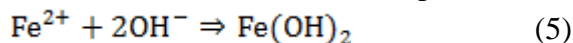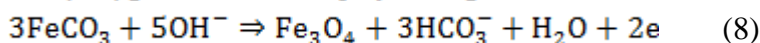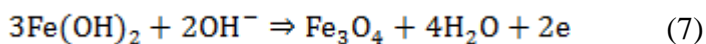$$HCO_3^- \Rightarrow CO_3^{2-} + H^+ \qquad (1)$$
Cathode reaction:
$$2H^+ + 2e \Rightarrow H_2 \qquad (2)$$

$$O_2 + 2H_2O + 4e \Rightarrow 4OH^- \qquad (3)$$

Anode reaction:

$$Fe + 2e \Rightarrow Fe^{2+} \qquad (4)$$

Formation of $Fe(OH)_2$ or $FeCO_3$ protective film [17]:

$$Fe^{2+} + 2OH^- \Rightarrow Fe(OH)_2 \qquad (5)$$

$$Fe^{2+} + CO_3^{2-} \Rightarrow FeCO_3 \qquad (6)$$

Thus, the corrosion product on the surface of X80 is mainly Fe $(OH)_2$ or $FeCO_3$ in a 0.5 mol $L^{-1}$ $NaHCO_3$ corrosion solution without $Cl^-$ present [18]. However, due to the poor stability and low density of the corrosion product, the product is easy to dissolve at higher polarization voltages, which yields an increase in the corrosion current density of X80. For this reason, the second anode current peak D emerges. This is mainly due to the formation of iron oxides, which make the passive film multi-layered, resulting in corresponding anodic peaks in the current [19-21]. As the anodic polarization continues in the 0.5 mol $L^{-1}$ $NaHCO_3$ solutions without $Cl^-$, the low-valence oxides formed at a low potential may be further oxidized, resulting in the formation of a more stable corrosion product film on the X80 surface, reducing the corrosion current density. The possible reaction is as follows [14, 22, 23]:

$$3Fe(OH)_2 + 2OH^- \Rightarrow Fe_3O_4 + 4H_2O + 2e \qquad (7)$$

$$3FeCO_3 + 5OH^- \Rightarrow Fe_3O_4 + 3HCO_3^- + H_2O + 2e \qquad (8)$$

The film resulting from a high potential is $Fe_2O_3$, which is produced by $Fe_3O_4$ undergoing the following reaction in aqueous solution [24, 25]:

$$2Fe_3O_4 + 2OH^- \Rightarrow 3Fe_2O_3 + H_2O + 2e \qquad (9)$$
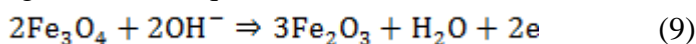
Although the stability of $Fe_2O_3$ is better than that of $Fe_3O_4$, the $Fe_2O_3$ crystal structure has a lower atomic space occupancy and poor compactness, which leads to the increase in the corrosion current density. As the polarized region of the sample surface is further covered by the stable passivation film, the anode current increases gradually. The appearance of the FG segment of the polarization curve in 0.5 mol $L^{-1}$ $NaHCO_3$ base solutions is mainly due to the exfoliation of loose corrosion products, resulting in a slight change in the corrosion current.

Once the polarization potential reaches point G, as the polarization potential continues to increase, the corrosion current is maintained at a nearly constant value. This qualitatively indicates that the X80 sample surface enters a stable passivation state at this point. When the polarization potential reaches point H, the surface of X80 begins to undergo transpassivation, which is mainly because the passive corrosion product film is further oxidized or ruptured, resulting in a corrosion current increase as the potential continues to rise [26]. This result shows that $HCO_3^-$ has a passivation ability in the corrosion solutions, but the ability is relatively weak. Prior research [27] has indicated that $HCO_3^-$ might form an oxide film with $Fe^{2+}$ to prevent anodic dissolution, or, on the contrary, $HCO_3^-$ might destroy the corrosion product film and cause pitting and stress corrosion cracking. After point H, the corrosion current density of X80 increases with the increase in the polarization potential, which may be due to the partial rupture or partial pitting of the passivation film on the specimen surface.

The anodic potential of the X80 electrode was strongly affected by the presence of corrosive chloride ions in 0.5 mol $L^{-1}$ $NaHCO_3$ solutions. With the increase of the chloride concentration in $NaHCO_3$ solutions, a stable passivation area does not appear on the X80 sample surface, but the

corrosion current density changes slightly when the anode potential is low (approximately -0.6 V). When the anode potential is shifted to a high value (approximately -0.2 V), the anode corrosion current increases rapidly, which indicates that the chloride ions have destroyed the X80 sample surface passivation film, and serious corrosion pitting appears on the polarized sample surface. As discussed previously [20, 28], the chloride ions lead to an increase in the probability of local rupture of the passivation film rather than the prevention of surface passivation.

The fitting parameters of the polarization curves can be obtained using the Tafel linear extrapolation method. The results of the fit are shown in Table 1. As seen from the Table 1, compared with the 0.5 mol $L^{-1}$ NaHCO$_3$ base solutions, there is an obvious increase in the $i_{cor}$ values when chloride ions are present. This increase in the $i_{cor}$ values may be due to chloride ion induction and activation of the specimen surface accelerating the corrosion of X80. It can also be noted from Figure 1 that chloride ions have a significant effect on the anodic reaction. The corrosion potential $E_{corr}$ values do not change significantly with the addition of various concentrations of chloride ions. When the concentration of chloride ions increased from 0.2 mol $L^{-1}$ to 0.4 mol $L^{-1}$ in the NaHCO$_3$ solutions, little influence on the active dissolution region of the polarization curve was observed. This is mainly due to the existence of corrosive chloride ions in solution, which induce and activate the X80 specimen surface and destroy the integrity of the corrosion product film.
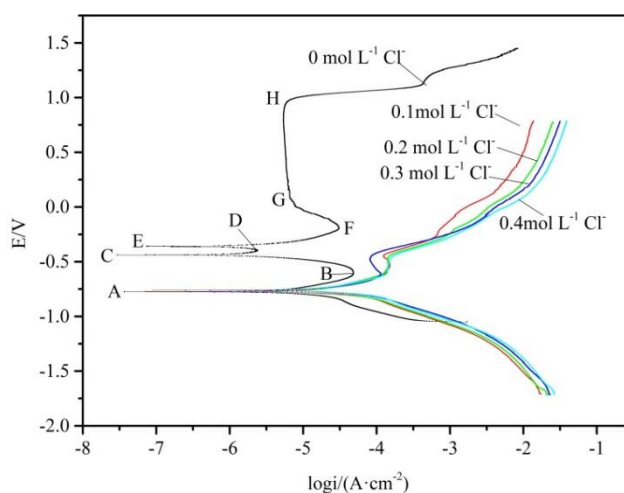


**Figure 1.** Polarization curves of X80 in 0.5 mol $L^{-1}$ NaHCO$_3$ corrosion solutions with different concentrations of chloride ions

**Table 2.** Corrosion kinetic parameters of X80 in 0.5 mol $L^{-1}$ NaHCO$_3$ solutions with and without the addition of various concentrations of chloride ions

| Cl$^-$ (mol $L^{-1}$) | $i_{cor}$ ($\mu$A cm$^{-2}$) | $b_a$ (V/dec) | $b_c$ (V/dec) | $E_{cor}$ (V vs Ag/AgCl) |
|---|---|---|---|---|
| 0 | 8.27 | 0.137 | -0.195 | -0.774 |
| 0.1 | 31.3 | 0.157 | -0.236 | -0.771 |
| 0.2 | 33.9 | 0.156 | -0.235 | -0.775 |
| 0.3 | 41.0 | 0.191 | -0.207 | -0.759 |
| 0.4 | 41.1 | 0.152 | -0.248 | -0.760 |

*3.2 Corrosion morphology*

At the same polarization potential and scanning rate, the surface morphology of the X80 pipeline steel after polarization in 0.5 mol L$^{-1}$ NaHCO$_3$ base solutions with and without different concentrations of chloride ions is shown in Figure 2. It can be seen from the figure that the surface morphology of the X80 specimen after polarization does not contain corrosion pits when no chloride ion was added to the 0.5 mol L$^{-1}$ NaHCO$_3$ foundation solution. Alwaranbi and Mao [29, 30] observed pitting corrosion for carbon steel in sodium bicarbonate solutions when the bicarbonate concentration was lower (0.01 mol L$^{-1}$ or 0.05 mol L$^{-1}$), and no pitting when the bicarbonate concentration was higher ($\geq$ 0.1 mol L$^{-1}$). When the concentration of chloride ions in the NaHCO$_3$ solution is 0.1 mol L$^{-1}$, many dense pits with smaller diameters form on the surface of the X80 samples. The number of active sites increases with the added NaCl, causing the acceleration of pitting corrosion because more chloride ions are adsorbed at the material surface [31, 32].
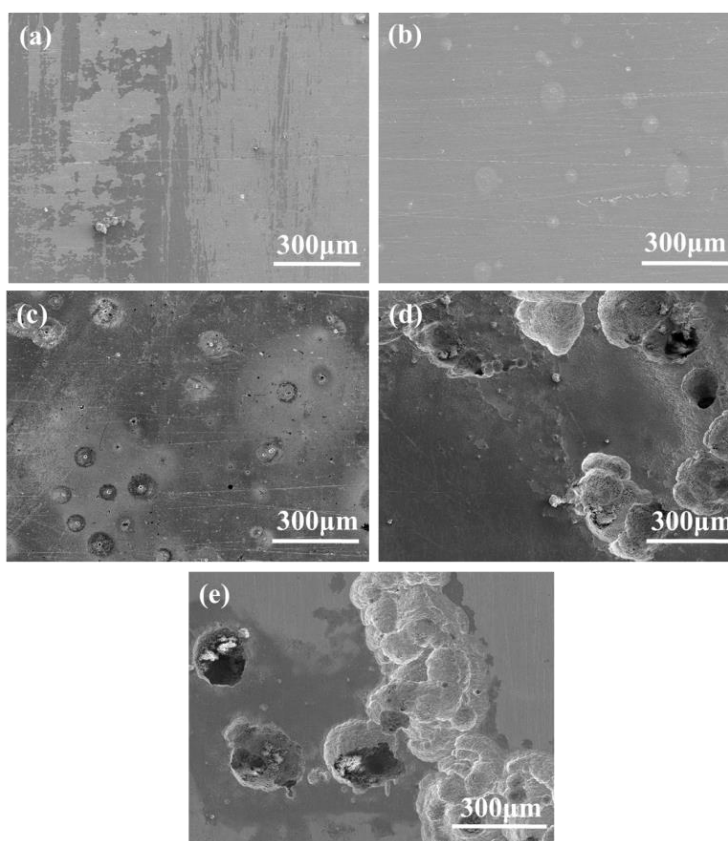


**Figure 2.** Corrosion morphology of X80 pipeline steel after polarization in 0.5 mol L$^{-1}$ NaHCO$_3$ solutions with different chloride ion concentrations: (a) 0.5 mol L$^{-1}$ NaHCO$_3$; (b) 0.5 mol L$^{-1}$ NaHCO$_3$+0.1 mol L$^{-1}$; (c) 0.5 mol L$^{-1}$ NaHCO$_3$+0.1 mol L$^{-1}$; (d) 0.5 mol L$^{-1}$ NaHCO$_3$+0.1 mol L$^{-1}$; (e) 0.5 mol L$^{-1}$ NaHCO$_3$+0.1 mol L$^{-1}$

With the increase in the chloride concentration, corrosion ensued upon the rupture of the passive film and proceeded inwardly along the corrosion pits [33]. Therefore, large-diameter corrosion pits were formed. As shown in Figure 2, with the increase in the chloride ion concentration, the

diameter of the corrosion pits on the sample increases gradually. When the concentration of chloride ion is 0.4 mol $L^{-1}$, the corrosion pits with 200 μm diameters are formed, and the corrosion pits become more concentrated and interconnected with each other. As the chloride ion concentration gradually increases in the 0.5 mol $L^{-1}$ NaHCO$_3$ solutions, the X80 sample surface shows more serious pitting corrosion because the passivation of X80 is gradually weakened by the chloride ions. This is mainly because with the increase in the chloride concentration, more chloride ions adsorb onto the X80 sample surface, causing more active sites to appear on the surface and accelerating the corrosion rate of the X80 [32].

### 3.3 Impedance measurements

The electrochemical properties of X80 steel in a 0.5 mol $L^{-1}$ NaHCO$_3$ solution with different concentrations of chloride ions obtained by means of electrochemical impedance measurements and typical Nyquist plots are illustrated in Figure 3. It can be found that the Nyquist plots of X80 at different concentrations of chloride ions displayed similar characteristics and that their impedance spectra did not change significantly. The low frequency semicircle is flattened for the X80 samples in 0.5 mol $L^{-1}$ NaHCO$_3$ solutions with different chloride ion concentrations.

The fitting of the impedance spectra was performed using ZSimpWin software. To obtain the best equivalent circuit, fitting of the experimental data was attempted using several models of the circuits. The equivalent circuit obtained with the best agreement between the experimental data and fitting results is shown in Figure 4. The specific fitting parameters of the equivalent circuit components are shown in Table 3, where $R_s$ is the solution resistance, $Q_f$ is the corrosion product capacitance, $R_f$ is the corrosion product resistance, $Q_{dl}$ is the electric double layer capacitance, and $R_{ct}$ is the charge transfer resistance. All impedance spectra show two time constants in these equivalent circuits. This may be due to the rapid oxidation of X80 in air to form an oxide film, resulting in a capacitive impedance loop in high frequency areas during impedance testing. The low-frequency loop shows that the corrosion processes of X80 pipeline steel were mainly controlled by a charge-transfer process, and the high-frequency arc was caused by the response of the corrosion products [34-37]. Moreover, with the increase in the chloride ion concentration, the semicircle diameter of the low-frequency region gradually decreases. Since the diameter of the semicircle is proportional to the charge-transfer resistance, it can be deduced that chloride ions are able to decrease the charge-transfer resistance and enhance the corrosion of the steel [38].

It has been reported that corrosion-product resistance and charge-transfer resistance decreases with the decrease in the thickness, compactness and stability of the corrosion products [34]. The impedance value is not only related to the formation of the $Fe^{3+}$ substance but is also a symbol of the continuous growth of the metal resistance layer. Moreover, the magnitude of the impedance value also indicates the protective effect of the passivation film. It is observed from Table 3 that the solution resistance values, $R_s$, the corrosion product resistance values, $R_f$, and the charge-transfer resistance values, $R_{ct}$, decrease for the X80 steel with further increases in the concentration of the chloride ions, which indicates that the corrosion resistance of X80 gradually decreases with the increase in the

chloride ion concentration. Therefore, it could be confirmed that with the increase in the chloride ion concentration, the corrosion rate of X80 increases and the coverage degree of the corrosion products decreases. Therefore, chloride ions are able to decrease the charge-transfer resistance and enhance the corrosion of X80 pipeline steel.
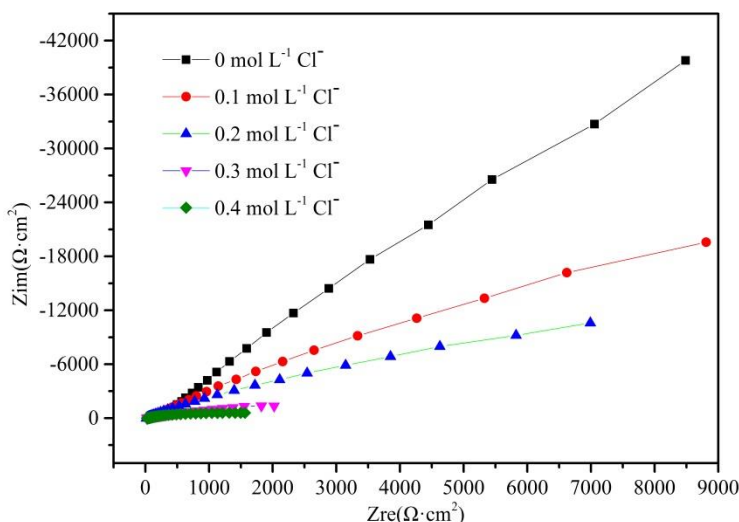


**Figure 3.** Nyquist plots of X80 in 0.5 mol L$^{-1}$ NaHCO$_3$ solutions with and without the addition of various concentrations of chloride ions
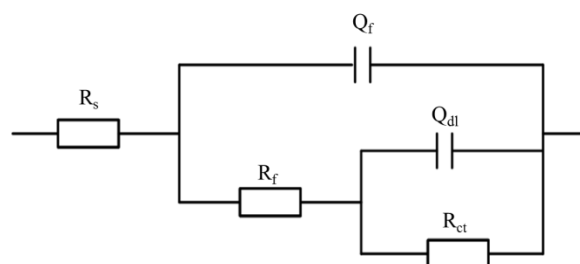


**Figure 4.** Equivalent electrical circuit model of X80 in 0.5 mol L$^{-1}$ NaHCO$_3$ solutions with and without the addition of various concentrations of chloride ions

**Table 3.** Electrochemical impedance fitting parameters for X80 in 0.5 mol L$^{-1}$ NaHCO$_3$ solutions with and without the addition of various concentrations of chloride ions

| Cl$^{-}$ (mol L$^{-1}$) | R$_s$ ($\Omega \cdot$cm$^2$) | R$_f$ ($\Omega \cdot$cm$^2$) | R$_{ct}$ ($\Omega \cdot$cm$^2$) | Q$_f$ (F$\cdot$cm$^2$) | Q$_{dl}$ (F$\cdot$cm$^2$) |
|---|---|---|---|---|---|
| 0 | 86.39 | 2018 | $2.199 \times 10^5$ | $3.306 \times 10^{-6}$ | $2.362 \times 10^{-5}$ |
| 0.1 | 42.34 | 1647 | $2.013 \times 10^5$ | $2.326 \times 10^{-5}$ | $2.013 \times 10^{-5}$ |
| 0.2 | 32.54 | 1475 | $1.802 \times 10^4$ | $3.164 \times 10^{-5}$ | $5.234 \times 10^{-5}$ |
| 0.3 | 28.38 | 599 | 4578 | $5.577 \times 10^{-5}$ | $3.619 \times 10^{-4}$ |
| 0.4 | 23.52 | 44 | 1277 | $2.533 \times 10^{-6}$ | $2.277 \times 10^{-6}$ |

## 4. CONCLUSIONS

(1) The dynamic potential polarization curves and electrochemical impedance spectra show that the increase in the $Cl^-$ concentration leads to a gradual decrease in the corrosion resistance of X80 steel. When no chloride ions are present in the 0.5 mol $L^{-1}$ $NaHCO_3$ corrosion solutions, X80 shows a passivation behaviour, and there are two anodic current peaks in the polarization curves. This shows that $HCO_3^-$ has a passivation ability in the solutions. With the increase in the concentration of chloride ions, the corrosion current density of the X80 steel increases gradually, and the corrosion of the X80 is accelerated; the samples do not undergo passivation in high-concentration chloride solutions. This indicates that the chloride ions lead to an increase in the probability of local rupture of the passivation film rather than the prevention of surface passivation.

(2) Under the same potential polarization, X80 shows varying degrees of pitting. The corrosion pits are larger in the $NaHCO_3$ base solutions with $Cl^-$ than in the $Cl^-$-free solutions. With the increase in the $Cl^-$ concentration, the diameter of the corrosion pits increases, and the pits gradually become centralized or even interconnected with each other. This is mainly due to the presence of corrosive chloride ions, which induce and activate the surface of the X80 sample, destroying the integrity of the corrosion product film and resulting in more severe pitting.

**References**

1. P. Liang, X. Li, C. Du and X. Chen, *Mater. Design*, 30 (2009) 1712.
2. B. He, C. H. Lu, P. J. Han and X. H. Bai, *Eng. Fail. Anal.*, 59 (2016) 410.
3. P. Wang, Z. Lv, S. Zheng, Y. Qi, J. Wang and Y. Zheng, *Int. J. Hydrogen Energ.*, 40 (2015) 11514.
4. K. Banerjee and U. K. Chatterjee, *Scripta Mater.*, 44 (2001) 213.
5. J. L. Alamilla, M. A. Espinosa-Medina and E. Sosa, *Corros. Sci.*, 51 (2009) 2628.
6. C. T. Lee, M. S. Odziemkowski and D. W. Shoesmith, *J. Electrochem. Soc.*, 153 (2006) B33.
7. Y. Wang, G. Cheng and Y. Li, *Corros. Sci.*, 111 (2016) 508.
8. Y. Wang, G. Cheng, W. Wu, Q. Qiao, Y. Li and X. Li, *Appl. Surf. Sci.*, 349 (2015) 746.
9. M. C. Li and Y. F. Cheng, *Electrochim. Acta*, 53 (2008) 2831.
10. M. M. El-Naggar, *Appl. Surf. Sci.*, 252 (2006) 6179.
11. Y. M. Zeng and J. L. Luo, *Electrochim. Acta*, 48 (2003) 3551.
12. R. W. Revie and R. R. Ramsingh, *Can. Metall. Quart.*, 22 (1983) 235.
13. S. Savoye, L. Legrand, G. Sagon, S. Lecomte, A. Chausse, R. Messina and P. Toulhoat, *Corros. Sci.*, 43 (2001) 2049.
14. Z. Lu, C. Huang, D. Huang and W. Yang, *Corros. Sci.*, 48 (2006) 3049.
15. F. F. Eliyan, E. Mahdi and A. Alfantazi, *Corros. Sci.*, 58 (2012) 181.
16. W. Zhao. H. Zhang. Y. Zou, *Int. J. Electrochem. Sci.*, 12 (2017) 679.
17. J. M. Santana-Casiano, M. González-Dávila and F. J. Millero, *Mar. Chem.*, 85(2004)27.

18. F. F. Eliyan, J. R. Kish and A. Alfantazi, *J. Mater. Eng.  Perfor.*, 24(2015)2473.
19. A. M. Riley and J. M. Sykes, *Electrochim. Acta*, 35(1990)35.
20. D. G. Li, Y. R. Feng, Z. Q. Bai, J. W. Zhu and M. S. Zheng, *Electrochim. Acta*, 52(2007)7877.
21. M. M. El-Naggar, *J. Appl.  Electrochem.*, 34(2004)911.
22. D. H. Davies and G. T. Burstein, *Corrosion*, 36 (1980) 416.
23. F. F. Eliyan and A. Alfantazi, Proc. From Eurocorr 2013, Paper No. *European Corrosion Congress 2013*, Portugal, 2013.
24. P. Hancock and J. E. O. Mayne, *J. Appl. Chem.*,9(1959)345.
25. J. G. N. Thomas, T. J. Nurse and R. Walker, *Brit. Corros. J.*, 5(1970)87.
26. B. Wang, T. Xin and Z. Gao, *Int. J. Electrochem. Sci*., 12(2017) 7205.
27. Z. Lu, C. Huang, D. Huang and W. Yang, *Corros. Sci.*, 48(2006)3049.
28. Y. F. Cheng, M. Wilmott and J. L.Luo, *Appl. Surf. Sci.*, 152(1999)161.
29. M. S. Alwaranbi, Chloride pitting corrosion of API X-80 and X-100 high strength low alloy pipeline steels in bicarbonate solutions, *Master dissertation available online*, (1999)University of British Columbia, Canada.
30. X. Mao, X. Liu and R. W. Revie, *Corros.  Sci.*, 50(1994)651.
31. J. Zhang and W. Zhao, *Surf. Interface Anal.* 43 (2011) 1018.
32. A. Rauf and E. Mahdi, *Int. J. Electrochem. Sci*., 7(2012)5692.
33. F. Xie, D. Wang, C. X. Yu, Y. Zong and M. Wu, *Int. J. Electrochem. Sci.*,12(2017)9565.
34. M. C. Yan, C. Sun, J. Xu and W. Ke, *Int. J. Electrochem. Sci.*, 10 (2015) 1762.
35. L. Hamadou, A. Kadri and N. Benbrahim, *Appl. Surf. Sci.*, 252 (2005) 1510.
36. S. X. Wang, D. X. Liu, N. Du,  Q. Zhao, S. Y. Liu and J. H. Xiao, *J. Int. J. Electrochem. Sci.*, 10(2015)4393.
37. F. F. Eliyan, E. S. Mahdi and A Alfantazi, *Corros. Sci.*, 58(2012)181.
38. X. Y.  Peng, Y. F. Cheng, *Can.  Metal. Quart.,* 53(2014)107.